Journal of Computational Physics 228 (2009) 4811–4822

Contents lists available at ScienceDirect

Journal of Computational Physics

journal homepage: www.elsevier.com/locate/jcp

Error control in the perfectly matched layer based multilevel fast multipole algorithm

Dries Vande Ginste *, Luc Knockaert, Daniël De Zutter

Department of Information Technology, Ghent University, Sint-Pietersnieuwstraat 41, B-9000 Gent, Belgium

ARTICLE INFO

Article history:
Received 23 June 2008
Received in revised form 12 February 2009
Accepted 24 March 2009
Available online 2 April 2009

Keywords:
Error controllability
Green function
Multilevel fast multipole algorithm
Perfectly matched layer
Layered medium

ABSTRACT

The development of efficient algorithms to analyze complex electromagnetic structures is of topical interest. Application of these algorithms in commercial solvers requires rigorous error controllability. In this paper we focus on the perfectly matched layer based multilevel fast multipole algorithm (PML-MLFMA), a dedicated technique constructed to efficiently analyze large planar structures. More specifically the crux of the algorithm, viz. the pertinent layered medium Green functions, is under investigation. Therefore, particular attention is paid to the plane wave decomposition for 2-D homogeneous space Green functions in very lossy media, as needed in the PML-MLFMA. The result of the investigations is twofold. First, upper bounds expressing the required number of samples in the plane wave decomposition as a function of a preset accuracy are rigorously derived. These formulas can be used in 2-D homogeneous (lossy) media MLFMAs. Second, a more heuristic approach to control the error of the PML-MLFMA's Green functions is presented. The theory is verified by means of several numerical experiments.

1. Introduction

During the past decades many efficient schemes for solving radiation and scattering by/from electrically large objects have been developed. The Fast Multipole Method (FMM) and the Multilevel Fast Multipole Algorithm (MLFMA) [1–4] are widely known. Application of the addition theorem leads to a diagonalization of the translator. This yields fast matrix-vector multiplications, as required in iterative solution schemes, and a significant reduction in memory requirements.

An important class of structures of topical interest are planar layered media problems, since they occur in many application areas such as RF/microwave electronics (monolithic microwave integrated circuits, planar antenna arrays, multilayered laminated printed circuit boards, etc.) and also in remote sensing (detection of buried objects, scattering of structures in the presence of stratified media, etc.). Another fast algorithm that is based on a diagonal factorization is the Fast Inhomogeneous Plane Wave Algorithm (FIPWA) [5]. This algorithm has been extended to layered medium problems [6,7] and is based on the spectral integral representation of the pertinent layered medium Green function, using propagating and evanescent plane waves. Also, perfectly matched layers (PMLs) [8,9] can be exploited in an analytical way to expand open layered medium Green functions in a series of modes [10,11]. Upon application of the PML's complex thickness paradigm, the series appear in a very natural way. Subsequently, these series can be combined with the FMM or with a MLFMA. Such dedicated fast algorithms for the efficient analysis of large layered medium problems, i.e. the PML-FMM and the PML-MLFMA, were recently developed [12,13], without having to compute cumbersome steepest descent path integrations.

The error controllability of the above described fast algorithms for layered media analysis is an important issue. On the one hand, it is crucial that the error sources can be clearly identified. On the other hand, heuristics need to be implemented

* Corresponding author. Tel.: +32 9 264 33 54; fax: +32 9 264 99 69.
E-mail address: dries.vande.ginste@intec.UGent.be (D. Vande Ginste).

0021-9991/$ - see front matter © 2009 Elsevier Inc. All rights reserved.
doi:10.1016/j.jcp.2009.03.034

that allow an easy automatic error setting of the fast algorithms. This makes them accessible for end-users who do not have a deep insight into the underlaying mathematics and physics of the algorithm, but are unknowingly using them, e.g. in RF/microwave design tools. Interesting studies of the error controllability of the FIPWA have already been published [14,15].

A thorough investigation of the error controllability of the PML-MLFMA is presented in this paper. The focus is on the crux of the algorithm, viz. the pertinent layered medium Green functions. These Green functions are expanded in a series of modes and each mode corresponds to a 2-D homogeneous space Green function. Hence, each mode can be decomposed into a set of plane waves, and therefore this plane wave decomposition has to be thoroughly investigated. Such error analysis has already been conducted for 2-D MLFMAs in lossless homogeneous background media [4,16]. In this paper, however, the focus is on the (quasi-)bandlimitedness of the 2-D radiation patterns in very lossy homogenous media, leading to two interesting results. Firstly, upper bounds for the required number of plane waves in a 2-D MLFMA in order to obtain a desired accuracy are rigorously derived. These formulas are immediately employable in 2-D MLFMAs to simulate scattering in very lossy background media. Secondly, a heuristic scheme, based on these upper bounds, is proposed to control the layered medium Green function's error. The usefulness of the upper bounds and of the heuristic approach are verified and demonstrated by means of several numerical experiments.

In Section 2 the PML-MLFMA is first briefly reviewed. Second, a qualitative discussion of its main error sources is presented. Third, we focus on the spectral content of the radiation patterns associated with the different modes, leading to new upper bounds that are applicable in general (lossy) 2-D homogeneous media. In Section 3 these formulas are numerically verified. Next, the error controllability of the complete expansion of the layered medium Green functions into modes and plane waves is demonstrated and an heuristic scheme is presented, which allows the presetting of a desired accuracy of the PML-MLFMA's Green functions. This is again illustrated by numerical experiments.

2. Analysis of the PML-MLFMA's error sources

In the sequel, all sources and fields are assumed time-harmonic with angular frequency ω and time dependencies $e^{j\omega t}$ are suppressed.

2.1. The layered medium Green functions

To analyze the error in the PML-MLFMA, we focus on the crux of the algorithm, i.e. the pertinent layered medium Green functions. Consider a microstrip configuration consisting of an infinite perfect electrically conducting (PEC)-backed substrate of thickness d, permittivity $\epsilon_1 = \epsilon_0\epsilon_r$, and permeability $\mu_1 = \mu_0\mu_r$; here ϵ_0 and μ_0 denote the permittivity and permeability of the air half-space $z > d$ above the substrate. The air half-space is closed by an PEC-backed perfectly matched layer (PML), which is equivalent to closing the half-space with a PEC plate placed at a *complex* distance $\tilde{D}$ above the substrate [10,11] (Fig. 1). At the substrate-air interface $z = d$, a source located at $\mathbf{r}' = x'\hat{\mathbf{x}} + y'\hat{\mathbf{y}} + d\hat{\mathbf{z}}$ resides in a source group of radius R

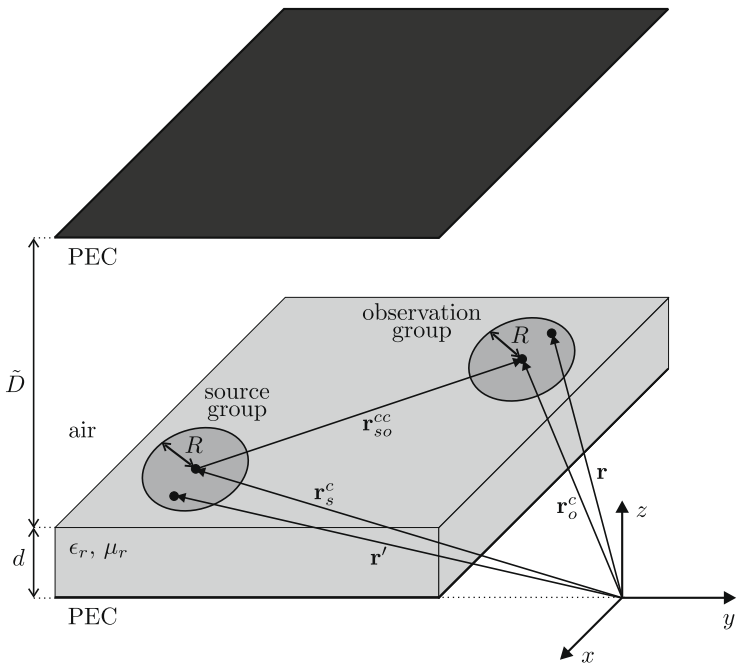

Fig. 1. Constellation of a source and an observation point on the substrate-air interface $z = d$ of a microstrip configuration.

centered about $\mathbf{r}_s^c$ and an observation point located at $\mathbf{r} = x\hat{\mathbf{x}} + y\hat{\mathbf{y}} + d\hat{\mathbf{z}}$ resides in an observation group of radius R centered about $\mathbf{r}_o^c$.

When only transverse-to-z currents at the substrate-air interface $z = d$ are considered, it is convenient to use the two scalar layered medium Green functions $G^A(\mathbf{r}|\mathbf{r}')$ and $G^V(\mathbf{r}|\mathbf{r}')$ – for the magnetic vector potential $\mathbf{A}(\mathbf{r})$ and the electric scalar potential $\phi(\mathbf{r})$, respectively – in a mixed potential integral equation (MPIE) formulation. This formulation, with two *scalar* Green functions instead of dyadics, corresponds to the *Formulation C* of [17]. These Green functions represent the magnetic potential and the electric potential at an observation point $\mathbf{r}$ caused by a dipole current at $\mathbf{r}'$, and classically, they are determined by evaluating the time-consuming Sommerfeld-type integrals [18]. However, by application of the PML-paradigm [10,11] the Green functions are expressed as a series of discrete TE- and TM-polarized modes, i.e.

$$G^A(\mathbf{r}|\mathbf{r}') = -\frac{j}{2}\sum_n \frac{H_0^{(2)}(\beta_{\mathrm{TE},n}|\mathbf{r}-\mathbf{r}'|)}{M^{\mathrm{TE}}(\beta_{\mathrm{TE},n})}, \tag{1}$$

$$G^V(\mathbf{r}|\mathbf{r}') = -\frac{j\omega^2}{2}\sum_n \frac{H_0^{(2)}(\beta_{\mathrm{TE},n}|\mathbf{r}-\mathbf{r}'|)}{\beta_{\mathrm{TE},n}^2 M^{\mathrm{TE}}(\beta_{\mathrm{TE},n})} + \frac{j}{2}\sum_n \frac{H_0^{(2)}(\beta_{\mathrm{TM},n}|\mathbf{r}-\mathbf{r}'|)}{\beta_{\mathrm{TM},n}^2 M^{\mathrm{TM}}(\beta_{\mathrm{TM},n})}. \tag{2}$$

Here, $H_0^{(2)}(\cdot)$ is the zeroth-order Hankel function of the second kind, and

$$M^{\mathrm{TE}}(\beta) = \frac{d}{\mu_1}\frac{1}{\sin^2\gamma_1 d} - \frac{\cot\gamma_1 d}{\mu_1\gamma_1} + \frac{\tilde{D}}{\mu_0}\frac{1}{\sin^2\gamma_0\tilde{D}} - \frac{\cot\gamma_0\tilde{D}}{\mu_0\gamma_0}, \tag{3}$$

$$M^{\mathrm{TM}}(\beta) = \frac{\epsilon_1\cot\gamma_1 d}{\gamma_1^3} + \frac{\epsilon_1 d}{\gamma_1^2\sin^2\gamma_1 d} + \frac{\epsilon_0\cot\gamma_0\tilde{D}}{\gamma_0^3} + \frac{\epsilon_0\tilde{D}}{\gamma_0^2\sin^2\gamma_0\tilde{D}}, \tag{4}$$

with $\gamma_m = \sqrt{k_m^2 - \beta^2}, m = 0, 1$, and $k_m = \omega\sqrt{\epsilon_m\mu_m}, m = 0, 1$. Theoretically, the summations in (1) and (2) extend over all TE- and TM-polarized modes, which are represented by their wavenumbers $\beta_{\mathrm{TX},n}, n = 1, \ldots, \infty$. Here and in what follows TX stands for TE and TM (X = E, M). For the microstrip configuration of Fig. 1, the TX-polarized modal wavenumbers $\beta_{\mathrm{TX},n}$ satisfy the following dispersion relation:

$$Y_1^{\mathrm{TX}}\cot(\gamma_1 d) + Y_0^{\mathrm{TX}}\cot(\gamma_0\tilde{D}) = 0, \tag{5}$$

with $Y_m^{\mathrm{TE}} = \frac{\gamma_m}{j\omega\mu_m}$ and $Y_m^{\mathrm{TM}} = \frac{j\omega\epsilon_m}{\gamma_m}, m = 0, 1$. It is important to stress that these wavenumbers are located in the fourth quadrant of the complex β-plane and that higher order modes have large negative imaginary parts. Hence, due to the decaying character of the Hankel functions, only a limited set of these modes is needed in practice.

Each Hankel function $H_0^{(2)}(\beta_{\mathrm{TX},n}|\mathbf{r}-\mathbf{r}'|)$ in the series (1) and (2) corresponds to the Green function of a 2-D homogeneous space with wavenumber $\beta_{\mathrm{TX},n}$. To construct a MLFMA, each such kernel is decomposed in terms of plane waves [4], i.e.

$$H_0^{(2)}(\beta_{\mathrm{TX},n}|\mathbf{r}-\mathbf{r}'|) \approx \sum_{q=-Q_{\mathrm{TX},n}}^{Q_{\mathrm{TX},n}} \left[e^{j\boldsymbol{\beta}_{\mathrm{TX},n}(\phi_q)\cdot(\mathbf{r}'-\mathbf{r}_s^c)}\; T_q(\beta_{\mathrm{TX},n}, |\mathbf{r}_{so}^{cc}|, \phi_{so}^{cc}) e^{-j\boldsymbol{\beta}_{\mathrm{TX},n}(\phi_q)\cdot(\mathbf{r}-\mathbf{r}_o^c)}\right], \tag{6}$$

where the diagonal translation operator T_q is defined as

$$T_q(\beta_{\mathrm{TX},n}, r, \phi) = \frac{1}{2Q_{\mathrm{TX},n}+1}\sum_{q'=-Q_{\mathrm{TX},n}}^{Q_{\mathrm{TX},n}} H_{q'}^{(2)}(\beta_{\mathrm{TX},n} r) e^{jq'\left(\phi-\phi_q-\frac{\pi}{2}\right)}, \tag{7}$$

with $\mathbf{r}_{so}^{cc} = \mathbf{r}_o^c - \mathbf{r}_s^c$, $\phi_{so}^{cc} = \arctan\left(\frac{\hat{\mathbf{y}}\cdot\mathbf{r}_{so}^{cc}}{\hat{\mathbf{x}}\cdot\mathbf{r}_{so}^{cc}}\right)$, and $\boldsymbol{\beta}_{\mathrm{TX},n}(\phi) = \beta_{\mathrm{TX},n}(\cos\phi\hat{\mathbf{x}} + \sin\phi\hat{\mathbf{y}})$. The sampling directions in (6) are uniformly distributed, i.e. $\phi_q = \frac{2q\pi}{2Q_{\mathrm{TX},n}+1}, q = -Q_{\mathrm{TX},n}, \ldots, Q_{\mathrm{TX},n}$, and $Q_{\mathrm{TX},n}$ depends on the modal wavenumber $\beta_{\mathrm{TX},n}$.

Substitution of (6) into (1) and (2) yields the Green functions, suitable for application in the PML-MLFMA. These Green functions can be interpreted as follows. The dipole source at $\mathbf{r}'$ causes radiation by the source group. This source group's radiation pattern is sampled into sets of $2Q_{\mathrm{TX},n}+1$ outgoing plane waves. There is one such set for each mode. Upon multiplication with the diagonal translation operator (7), each set is converted into a set of $2Q_{\mathrm{TX},n}+1$ incoming plane waves arriving at the observation group. There is one such set for each mode and there is no coupling between sampling directions or modes. The incoming plane waves are evaluated at the observation point $\mathbf{r}$. By using the proper mode-dependent weighting factors, the magnetic vector potential and the electric scalar potential in the layered medium radiated by the dipole source, viz. the pertinent layered medium Green functions, are computed.

2.2. Qualitative discussion of the PML-MLFMA's main error sources

In this subsection, the three most significant sources of error in the PML-MLFMA are briefly discussed.

The first error source lies in the PML-paradigm. The convergence of the series has been detailed in [10,11]. We here repeat the main findings that are relevant for the further reading of this paper. For a certain distance $|\mathbf{r}-\mathbf{r}'|$ between the source and the observation point, the limited number of modes used in the algorithm determines the precision of the modal expansions (1) and (2). On the one hand, for small values of $|\mathbf{r}-\mathbf{r}'|$ the series become impractical, since in that case too many modes are

needed. Hence, when used in the PML-MLFMA, the Green functions are preferably not expanded into modes for evaluation of the self-patch interaction. In the PML-MLFMA, as in most MLFMAs, self-patch interactions are handled by a classical evaluation technique, and therefore, this error is not further discussed. On the other hand, to obtain a preset accuracy a decreasing number of modes is needed for increasing distance $|\mathbf{r}-\mathbf{r}'|$. This property is exploited in the PML-MLFMA and illustrated in Section 3.3.

The second source of error is due to the diagonal translation operator (7), which is the case for all MLFMAs. The absolute value of the qth order Hankel function of the second kind increases faster than exponentially with q when this order is larger than the absolute value of its argument $|\beta_{\mathrm{TX},n}\mathbf{r}_{so}^{cc}|$. As the machine precision is limited, this causes numerical errors. For increasing group size R, an increasing number of samples $2Q_{\mathrm{TX},n}+1$ has to be used (see further). Hence, the precision of the translation should be controlled by selecting a large enough buffer between the source group and the observation group, i.e. by choosing the translation distance $|\mathbf{r}_{so}^{cc}|$ large enough with respect to the group size R. In this context the term 'well-separateness' is often used. Here, we adopt the concept of 'buffer groups'. This is the minimal distance, divided by $2R$, between a source group and an observation group below which the expansion (6) is not used. The choice of the number of buffer groups has been discussed and demonstrated abundantly in [16].

The third source of error in the PML-MLFMA is the sampling of the radiation patterns for each mode. According to Nyquist's theorem, a perfectly bandlimited radiation pattern can be reconstructed from its samples without loss of accuracy. However, the radiation patterns as described above are not perfectly bandlimited. Also, as stated before, for each mode, the number of samples $2Q_{\mathrm{TX},n}+1$ depends on the wavenumber $\beta_{\mathrm{TX},n}$. Because of its particular importance in the PML-MLFMA, the spectral content of the radiation patterns for each mode is rigorously investigated in the next section. Of course, apart from *analytical* considerations w.r.t. the sampling error, the decomposition into plane waves also induces *numerical* errors in the PML-MLFMA. This is illustrated in Section 3.2.

2.3. Spectral content of the radiation patterns

For a given wavenumber $\beta_{\mathrm{TX},n}$, the spectral content of the radiation pattern only depends on the size R of the groups. It has been shown [4,19] that, if a large enough buffer between the source group and observation group is used, any desired accuracy for the plane wave decomposition (6) can be achieved, up to machine precision. Therefore, the number of samples used in the plane wave decomposition has to be chosen as

$$Q_{\mathrm{TX},n} = 2\beta_{\mathrm{TX},n}R + 1.8d_0^{2/3}(2\beta_{\mathrm{TX},n}R)^{1/3}, \tag{8}$$

where the constant d_0 is the desired number of digits of accuracy of the plane wave decomposition. Eq. (8) is known as the refined excess bandwidth formula. Of course, in its form (8), this formula is only valid for real wavenumbers $\beta_{\mathrm{TX},n}$. Note, however, that in the PML-MLFMA, the Green function is written as a sum of many modes and that all modal wavenumbers $\beta_{\mathrm{TX},n}$ are located in the fourth quadrant of the complex β-plane. Especially higher order modes can have significant imaginary parts and hence, formula (8) may no longer be valid.

In the sequel it is shown that for each mode with modal wavenumber $\beta_{\mathrm{TX},n}$, the radiation pattern is *quasi-bandlimited* (see further), allowing to sample these radiation patterns. In the PML-MLFMA, the required number of samples $2Q_{\mathrm{TX},n}+1$ can be determined by analyzing the bandwidth (spectral content) of the total radiation pattern

$$\mathcal{R}(\phi) = e^{+j\boldsymbol{\beta}_{\mathrm{TX},n}(\phi)\cdot\left[\left(\mathbf{r}'-\mathbf{r}_s^c\right)-\left(\mathbf{r}-\mathbf{r}_o^c\right)\right]}. \tag{9}$$

$\mathcal{R}(\phi)$ is periodic with period 2π on the real axis ($\phi\in\mathcal{R}$). It can be expanded in its Fourier series

$$\mathcal{R}(\phi) = \sum_{q=-\infty}^{+\infty} c_q e^{-jq\phi}, \tag{10}$$

where

$$c_q = \frac{1}{2\pi}\int_0^{2\pi}\mathcal{R}(\phi)e^{jq\phi}d\phi \tag{11}$$

$$= \frac{1}{2\pi}\int_0^{2\pi} e^{j\beta_{\mathrm{TX},n}\Delta\cos(\phi-\alpha)}e^{jq\phi}d\phi, \tag{12}$$

with $\Delta = |(\mathbf{r}'-\mathbf{r}_s^c)-(\mathbf{r}-\mathbf{r}_o^c)|$ and $\tan\alpha = \frac{\hat{\mathbf{y}}\cdot\left[\left(\mathbf{r}'-\mathbf{r}_s^c\right)-\left(\mathbf{r}-\mathbf{r}_o^c\right)\right]}{\hat{\mathbf{x}}\cdot\left[\left(\mathbf{r}'-\mathbf{r}_s^c\right)-\left(\mathbf{r}-\mathbf{r}_o^c\right)\right]}$. Truncating this series, we obtain

$$\mathcal{R}(\phi) = \sum_{q=-Q_{\mathrm{TX},n}}^{+Q_{\mathrm{TX},n}} c_n e^{-jq\phi} + S_{Q_{\mathrm{TX},n}}(\phi), \tag{13}$$

and the truncation error is given by

$$S_{Q_{\mathrm{TX},n}}(\phi) = \sum_{q=Q_{\mathrm{TX},n}+1}^{+\infty}\left(c_q e^{-jq\phi} + c_{-q}e^{jq\phi}\right). \tag{14}$$

For $\phi \in \mathcal{R}$ we have

$$|S_{Q_{TX,n}}(\phi)| \leqslant R_{Q_{TX,n}} = \sum_{q=Q_{TX,n}+1}^{+\infty} \left(|c_q| + |c_{-q}|\right). \tag{15}$$

Using Bessel's first integral [20] for integer q,

$$J_q(z) = \frac{1}{\pi}\int_0^{\pi} \cos(q\theta - z\sin\theta)d\theta = \frac{1}{2\pi}\int_0^{2\pi} e^{jq\theta}e^{-jz\sin\theta}d\theta, \tag{16}$$

it is readily seen that

$$R_{Q_{TX,n}} = 2\sum_{q=Q_{TX,n}+1}^{+\infty} |J_q(\beta_{TX,n}\Delta)|. \tag{17}$$

In [21] it is shown that

$$|J_q(z)| \leqslant \frac{\left|\frac{z}{2}\right|^q e^{|\Im(z)|}}{\Gamma(q+1)} \text{ for } q > -\frac{1}{2}, \tag{18}$$

where $\Im(z)$ is the imaginary part of z and $\Gamma(z)$ is the Gamma function [20]. Introducing the incomplete Gamma function $\Gamma(z,u) \equiv \int_u^{\infty} t^u e^{-t}dt$ [20], and putting $a = |\frac{\beta_{TX,n}\Delta}{2}|$ and $b = |\Im(\beta_{TX,n}\Delta)|$, a first upper bound of $R_{Q_{TX,n}}$ is found:

$$R_{Q_{TX,n}} \leqslant 2e^b \sum_{q=Q_{TX,n}+1}^{+\infty} \frac{a^q}{q!} \tag{19}$$

$$= 2e^{a+b}\left(1 - \frac{\Gamma(Q_{TX,n}+1, a)}{\Gamma(Q_{TX,n}+1)}\right). \tag{20}$$

In (19) and (20) the astute reader will recognize the Erlang or cumulative Poisson distribution [22]. Substituting the integral definitions of the Gamma function and the incomplete Gamma function into (20) yields

$$R_{Q_{TX,n}} \leqslant 2\ e^{a+b}\ \frac{\int_0^a t^{Q_{TX,n}}e^{-t}\ dt}{\Gamma(Q_{TX,n}+1)}. \tag{21}$$

Since $a \geqslant 0$, we obtain

$$\int_0^a t^{Q_{TX,n}}e^{-t}\ dt \leqslant \int_0^a t^{Q_{TX,n}}\ dt = \frac{a^{Q_{TX,n}+1}}{Q_{TX,n}+1}, \tag{22}$$

which majorizes (21) (and thus $|S_{Q_{TX,n}}(\phi)|$):

$$R_{Q_{TX,n}} \leqslant 2\ e^{a+b}\ \frac{a^{Q_{TX,n}+1}}{(Q_{TX,n}+1)\Gamma(Q_{TX,n}+1)} = 2\ e^{a+b}\ \frac{a^{Q_{TX,n}+1}}{(Q_{TX,n}+1)!}. \tag{23}$$

The following double inequality [23]

$$\sqrt{2\pi}\ m^{m+1/2}\ e^{-m+1/(12m+1)} < m! < \sqrt{2\pi}\ m^{m+1/2}\ e^{-m+1/(12m)} \tag{24}$$

provides bounds for the factorial function. This implies

$$R_{Q_{TX,n}} \leqslant \frac{2\ e^{a+b}}{\sqrt{2\pi(Q_{TX,n}+1)}\ e^{1/(12Q_{TX,n}+13)}}\left(\frac{Q_{TX,n}+1}{ae}\right)^{-(Q_{TX,n}+1)}. \tag{25}$$

It is clear that for $Q_{TX,n} \geqslant 0$

$$\sqrt{Q_{TX,n}+1}\ e^{1/(12Q_{TX,n}+13)} \geqslant e^{1/13} > 1. \tag{26}$$

Hence another upper bound is obtained as

$$R_{Q_{TX,n}} < \sqrt{\frac{2}{\pi}}\ e^{a+b}\left(\frac{Q_{TX,n}+1}{ae}\right)^{-(Q_{TX,n}+1)}. \tag{27}$$

The right hand side of (27) has a maximum for $Q_{TX,n} = a - 1$. For increasing $Q_{TX,n}$, larger than $a - 1$, the truncation error decreases *faster than exponentially* to zero, and hence, it can be stated that the spectral content of the radiation pattern $\mathcal{R}(\phi)$ is *quasi-bandlimited*, allowing to sample it with controllable accuracy.

2.4. A simple upper bound for the number of samples $2Q_{TX,n}+1$

In the previous section upper bounds have been derived, expressing the truncation error as a function of the number of samples. A first appropriate expression for the truncation error is (20) (the Erlang distribution). Unfortunately, there does not exist an analytical inverse of this cumulative distribution. Expressing $2Q_{TX,n}+1$ as a function of a desired accuracy, as is also achieved with the excess bandwidth formula (8), is of practical use. Say an absolute accuracy $\mathcal{E}$ for the truncation as proposed in (13) is desired. A second upper bound for the truncation error is given by (27), which we now demand to be smaller than $\mathcal{E}$, i.e.

$$\sqrt{\frac{2}{\pi}}\, e^{a+b}\left(\frac{Q_{TX,n}+1}{ae}\right)^{-(Q_{TX,n}+1)} < \mathcal{E}. \tag{28}$$

The following notation is introduced

$$\mathcal{E}' = -\ln\mathcal{E} - \frac{1}{2}\ln\frac{\pi}{2} + a + b. \tag{29}$$

Since $a \geqslant 0$ and $b \geqslant 0$, $\mathcal{E}'$ is certainly positive for $\mathcal{E} < \sqrt{\frac{2}{\pi}}$. Of course, we can always aim at a much lower $\mathcal{E}$. Therefore, it is safe to transform (28) into

$$\frac{\mathcal{E}'}{Q_{TX,n}+1}\, e^{\frac{\mathcal{E}'}{Q_{TX,n}+1}} < \frac{\mathcal{E}'}{ae}. \tag{30}$$

The Lambert-W function $W(z)$ [24] is the inverse function of z, with z defined as $z \equiv W(z)e^{W(z)}$. $W(z)$ is positive and strictly increasing for $z > 0$. Applying this definition of $W(z)$ yields

$$\frac{\mathcal{E}'}{Q_{TX,n}+1} < W\left(\frac{\mathcal{E}'}{ae}\right), \tag{31}$$

or finally, the accuracy $\mathcal{E}$ is met by demanding that

$$Q_{TX,n} > \frac{\mathcal{E}'}{W\left(\frac{\mathcal{E}'}{ae}\right)} - 1. \tag{32}$$

3. Experimental verification and error controllability

3.1. Theoretical accuracy of the plane wave decomposition (6)

Consider the constellation of Fig. 1 with $\mathbf{r}' = (0, R, d)$, $\mathbf{r}_s^c = (0, 0, d)$, $\mathbf{r}_o^c = (2R(B+1), 0, d)$, and $\mathbf{r} = (2R(B+1), -R, d)$. So, the source and observation point are located on the edge of the source and observation group, respectively. The parameter B determines the number of buffer groups between the source and the observation group. A top view of this constellation is shown in Fig. 2.

In this section, the theoretical accuracy of the plane wave decomposition (6) is analyzed, using *Mathematica*® *5.1*. Hence, numerical errors do not come into play. We consider a single mode and denote its wavenumber as $\beta_{TX,n} = \beta = |\beta|e^{-j\theta}, \theta : 0 \to \frac{\pi}{2}$. In this section, the subscript on the number of samples $2Q+1$ is omitted for simplicity. Furthermore, consider $|\beta|R = 3$ and $B = 5$. Fig. 3 shows the relative error of the plane wave decomposition (6) with respect to the Hankel function, i.e.

$$\left|\frac{H_0^{(2)}(\beta|\mathbf{r}-\mathbf{r}'|) - \sum_{q=-Q}^{Q}\left[e^{j\boldsymbol{\beta}(\phi_q)\cdot(\mathbf{r}'-\mathbf{r}_s^c)}\; T_q(\beta, |\mathbf{r}_{so}^{cc}|, \phi_{so}^{cc}) e^{-j\boldsymbol{\beta}(\phi_q)\cdot(\mathbf{r}-\mathbf{r}_o^c)}\right]}{H_0^{(2)}(\beta|\mathbf{r}-\mathbf{r}'|)}\right|, \tag{33}$$

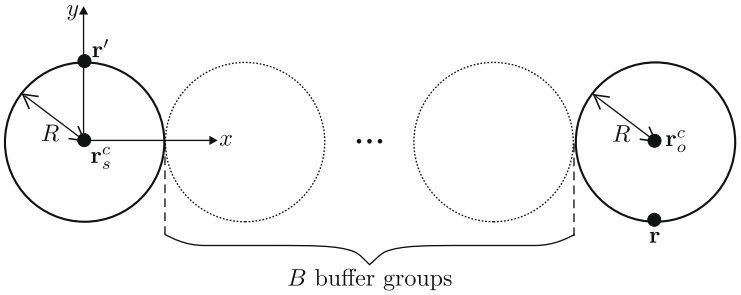

Fig. 2. Top view of the constellation.

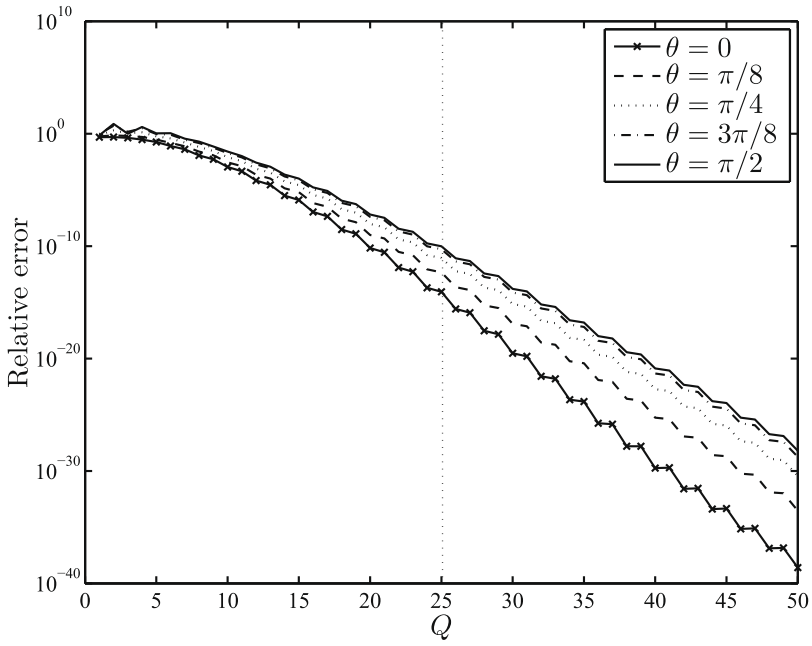

Fig. 3. Theoretical accuracy of the plane wave decomposition (6) for an increasing sampling rate and for five different values of θ.

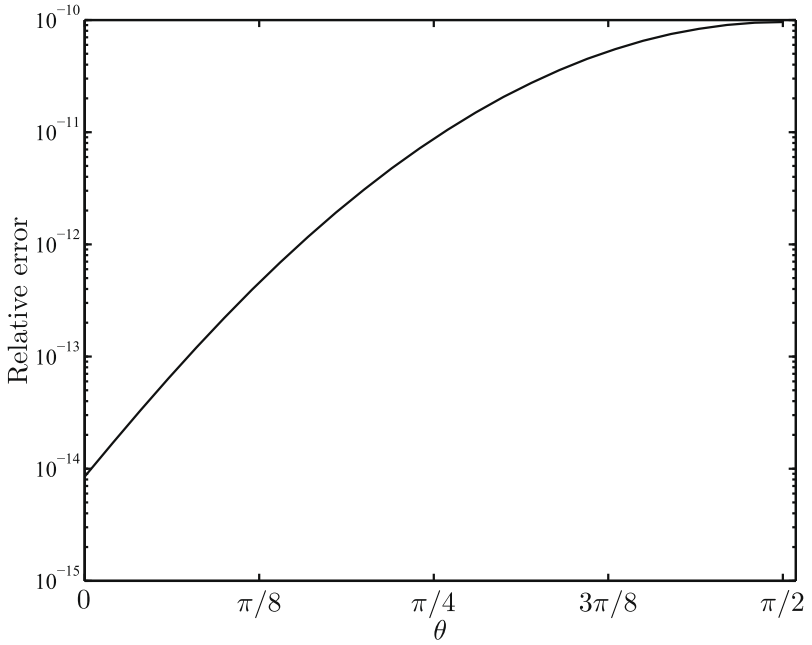

Fig. 4. Theoretical accuracy of the plane wave decomposition (6) for increasing losses θ and at a fixed sampling rate, i.e. $2Q + 1 = 51$.

as a function of the number of samples $2Q + 1$ and for five different values of θ. As in *Mathematica*® the accuracy is not limited to, e.g., double precision (16 digits), any desired accuracy for the plane wave decomposition can be achieved by increasing Q. The staircase convergence, clearly visible in Fig. 3, is most prominent for the particular constellation of Fig. 2 where the vectors $\left[(\mathbf{r}' - \mathbf{r}_s^c) - (\mathbf{r} - \mathbf{r}_o^c)\right]$ and $(\mathbf{r}_o^c - \mathbf{r}_s^c)$ are perpendicular and this is less pronounced when these vectors are parallel. From Fig. 3, it can also be concluded that the relative error increases for increasing θ. In Fig. 4, again it is demonstrated that for a fixed number of samples $2Q + 1 = 51$ (see also $Q = 25$ in Fig. 3), the accuracy decreases when θ increases, i.e. when the medium becomes more and more lossy, up to the point where both the medium's permittivity and permeability are purely imaginary numbers and β is located on the negative imaginary axis ($\theta = \pi/2$). Strongly evanescent modes can exhibit such behavior.

Table 1
Estimates Q, obtained by using (8), (20), and (32), leading to an actual number of digits of accuracy for the plane wave decomposition (6), as a function of a desired number of digits of accuracy d_0 and for a varying parameter θ.

Desired digits of accuracy d_0	θ	Estimated Q, using (8)	Actual digits of accuracy, following (8)	Estimated Q, using (20)	Actual digits of accuracy, following (20)	Estimated Q, using (32)	Actual digits of accuracy, following (32)
3	0	13	4.55	12	4.17	15	5.90
	$\pi/8$	13	4.00	15	5.20	18	7.55
	$\pi/4$	13	3.46	17	5.77	20	8.04
	$3\pi/8$	13	3.08	19	6.46	21	7.70
	$\pi/2$	13	***2.95***	19	6.27	21	7.48
6	0	17	7.35	16	6.96	19	8.91
	$\pi/8$	17	6.50	19	7.88	21	9.31
	$\pi/4$	17	***5.77***	21	8.33	23	9.67
	$3\pi/8$	17	***5.27***	22	8.69	24	10.02
	$\pi/2$	17	***5.10***	23	8.73	25	10.02
9	0	21	10.55	20	10.17	22	11.91
	$\pi/8$	21	9.31	22	10.51	25	12.34
	$\pi/4$	21	***8.33***	24	10.80	26	12.23
	$3\pi/8$	21	***7.70***	25	10.28	28	12.74
	$\pi/2$	21	***7.48***	26	11.08	28	12.43
12	0	24	13.72	24	13.72	26	15.59
	$\pi/8$	24	12.07	26	13.66	28	15.27
	$\pi/4$	24	***10.80***	27	12.47	29	13.92
	$3\pi/8$	24	***10.02***	29	12.98	31	14.36
	$\pi/2$	24	***9.75***	29	12.67	31	14.03
15	0	26	15.59	27	15.93	29	17.84
	$\pi/8$	26	***13.66***	29	15.51	31	17.13
	$\pi/4$	26	***12.23***	30	15.16	32	16.65
	$3\pi/8$	26	***11.37***	32	15.55	33	15.77
	$\pi/2$	26	***11.08***	32	15.19	34	16.59

It was already suggested in [25] – for a 3-D configuration – that replacing β by its absolute value $|\beta|$ in the excess bandwidth formula (8) does not provide an accurate estimate for the number of samples in a lossy medium and that Q should be chosen slightly larger to maintain the same level of accuracy for moderate losses. The above derived formulas (20) and (32), quantify this statement since they explicitly include the losses (via the parameter b), albeit not exactly (Eqs. (20) and (32) only provide upper bounds). In Table 1 the estimates for Q are given for several desired relative accuracies, expressed as the desired number of digits of accuracy d_0, and for a varying parameter θ by using three different estimates: (i) the excess bandwidth formula (8), with β replaced by its absolute value $|\beta|$, (ii) the estimate (20), which can be inverted in *Mathematica*® by using a root finding procedure, as such expressing Q as a function of the desired accuracy, and (iii) the upper bound (32). Also, the actual relative accuracy, expressed as the actual number of digits of accuracy, obtained by using these three estimates, is presented in Table 1. From this table it can be concluded that:

- When β is real ($\theta = 0$), the excess bandwidth formula (8) provides a good estimate for Q, yielding the desired number of digits of accuracy.
- When β is located in the fourth quadrant of the complex β-plane ($0 < \theta \leqslant \pi/2$), the excess bandwidth formula (8) – where β is replaced by $|\beta|$ – yields an underestimation of Q, often leading to a lower number of digits of accuracy than what was required. These values are indicated in bold italic in the table.
- Using Eq. (20) always leads to the required relative error.
- Using Eq. (32) always leads to the required relative error too. On the one hand, (32) sometimes overestimates the number of samples $2Q + 1$, leading to a few digits of accuracy more than what is desired. On the other hand, and in contrast with (20), a root finding procedure to determine Q is not required.

3.2. Numerical accuracy of the plane wave decomposition (6)

Again, the constellation as in the previous section (Fig. 2) is used. But now the accuracy of the plane decomposition (6) is tested numerically in *Matlab*® *7.4*. Hence, the maximum achievable precision is limited to 16 digits (i.e. double precision). Fig. 3 is reproduced with this limited accuracy, which leads to Fig. 5. First, consider the curve for the lossless case $\theta = 0$. This characteristic numerical behavior of the accuracy as a function of Q has been abundantly discussed in the past [16]. A region with controllable accuracy can be identified for which the error decreases by increasing Q, according to the excess bandwidth formula (8). Then, a plateau is reached, because the smallest relative error is limited to machine precision (here 16 digits). For high Q, the relative error increases again, for reasons explained in Section 2.2, i.e. the argument of the Hankel functions in the translator operator (7) becomes smaller than the order, leading to numerical round-off errors. This phenomenon has also been discussed in [16]. The extent of plateau for which the maximum accuracy is reached can be enlarged by increasing the buffer. In Fig. 5, the buffer is $B = 5$, which is a relatively small buffer. Next, for complex β ($0 < \theta \leqslant \pi/2$), the accuracy is lower,

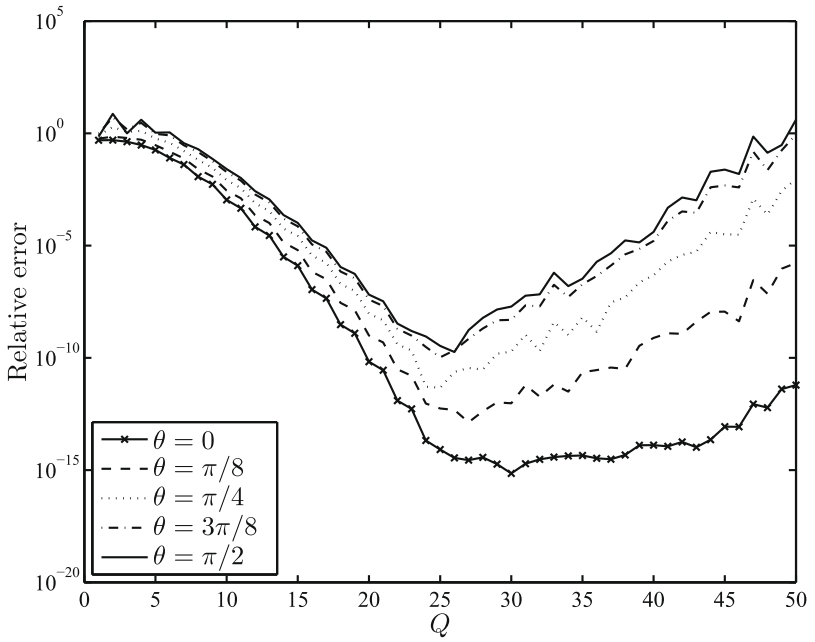

Fig. 5. Numerical accuracy of the plane wave decomposition (6) for an increasing sampling rate and for five different values of θ.

as expected (see Section 3.1). However, an extra numerical error is induced as well. For real wavenumbers β, the modulus of the radiation pattern is one for every sampling angle, i.e. $|\mathcal{R}(\phi_q)| = 1$, $q = -Q, \ldots, Q$. For complex β, Q samples will exhibit a decaying exponential behavior and the other Q samples correspond to increasing exponentials. Summation of increasing and decreasing exponentials unavoidably leads to numerical errors, as can be seen in Fig. 5. Increasing the buffer B leads to better results, but still 16 digits of accuracy cannot always be reached. E.g., for $B = 15$ and $\theta = \pi/2$, the minimal attainable relative error is 10^{-12}.

Some modes of the layered medium Green functions correspond to complex wavenumbers with large negative imaginary parts. So, the question arises, is a controllable accuracy attainable in the PML-MLFMA? The answer is yes, as will be shown in the next section.

3.3. Numerical accuracy of the layered medium Green functions $G^A(\mathbf{r}|\mathbf{r}')$ and $G^V(\mathbf{r}|\mathbf{r}')$

Consider the constellation of Fig. 1. For a 'realistic substrate', with e.g. $\epsilon_r > 1$ and $\mu_r = 1$ and/or with multiple dielectric layers, the Green functions are classically computed by numerically evaluating Sommerfeld-type integrals. However, to have an exact reference solution, an air-substrate is used here, as for this special configuration the layered medium Green functions are analytically known. The air-substrate has a relative permittivity $\epsilon_r = 1$, a relative permeability $\mu_r = 1$, and a thickness $d = 1$ mm. The structure is closed by a PEC-backed PML, i.e. a PEC is placed at $z = d + \tilde{D}$, with $\tilde{D} = 0.25e^{-j\pi/4}$ m. The angular frequency is fixed at $\omega = 2\pi 10^9$ Hz. For the air-substrate, the layered medium Green functions are obtained by solving a free space problem with two elementary dipole sources, one placed at $\mathbf{r}' = (x', y', d)$ and an image source situated at $(x', y', -d)$, yielding

$$G^A(|\mathbf{r} - \mathbf{r}'|) = \frac{\mu_0}{4\pi}\left(\frac{e^{-jk_0|\mathbf{r}-\mathbf{r}'|}}{|\mathbf{r} - \mathbf{r}'|} - \frac{e^{-jk_0\sqrt{|\mathbf{r}-\mathbf{r}'|^2+4d^2}}}{\sqrt{|\mathbf{r} - \mathbf{r}'|^2 + 4d^2}}\right), \tag{34}$$

$$G^V(|\mathbf{r} - \mathbf{r}'|) = \frac{1}{4\pi\epsilon_0}\left(\frac{e^{-jk_0|\mathbf{r}-\mathbf{r}'|}}{|\mathbf{r} - \mathbf{r}'|} - \frac{e^{-jk_0\sqrt{|\mathbf{r}-\mathbf{r}'|^2+4d^2}}}{\sqrt{|\mathbf{r} - \mathbf{r}'|^2 + 4d^2}}\right), \tag{35}$$

as such providing an accurate reference to test the error controllability. Conveniently, the wavenumbers are analytically known for this configuration:

$$\beta_{\mathrm{TE},n} = \beta_{\mathrm{TM},n} = \sqrt{k_0^2 - \left(\frac{n\pi}{d + \tilde{D}}\right)^2}, \quad n = 1, \ldots, \infty. \tag{36}$$

From (36), it is immediately clear that the modal wavenumbers can have large negative imaginary parts, which leads to higher sampling rates compared to real wavenumbers and which also introduces numerical errors, as explained before. Fortunately, in the decompositions (1) and (2), the relative importance of high order modes decreases with increasing order n.

This is due to the decaying character of the Hankel functions $H_0^{(2)}(\beta_{\mathrm{TX},n}|\mathbf{r}-\mathbf{r}'|)$. In the series (1) and (2), for larger values of $|\mathbf{r}'-\mathbf{r}|$ only a few modes are needed, for small values of $|\mathbf{r}'-\mathbf{r}|$ many modes are needed. This property is exploited in the implementation of the PML-MLFMA and demonstrated below. Instead of using formulas as (8), (20), or (32) for each mode separately, the relative importance of the different terms in (1) and (2) is taken into account. The following heuristic approach is implemented to control the error:

(i) A global accuracy for the Green functions is chosen. This desired accuracy is characterized by d_0, i.e. the number of digits of accuracy w.r.t. the actual open space layered medium Green functions, in this case (34) and (35).
(ii) A maximum numbers of TE- and TM-polarized modes M for the series expansions (1) and (2) is selected. This number M determines the maximum achievable accuracy at a certain distance $|\mathbf{r}-\mathbf{r}'|$ [10,11]. Of course, the relative error 10^{-d_0} has to be attainable by using M modes.
(iii) Next, the required sampling rates are determined. Therefore, for each mode – represented by its wavenumber $\beta_{\mathrm{TX},n}, n=1,\ldots,M$ – the minimal number of samples $2Q_{\mathrm{TX},n}+1$ for which the condition

$$\left|\left(\sum_{q=-Q_{\mathrm{TX},n}}^{Q_{\mathrm{TX},n}} C_q\right) - H_0^{(2)}(\beta_{\mathrm{TX},n}|\mathbf{r}-\mathbf{r}'|)\right| < \frac{10^{-d_0}}{M}\left|H_0^{(2)}(\beta_{\mathrm{TM},1}|\mathbf{r}-\mathbf{r}'|)\right|, \tag{37}$$

with

$$C_q = e^{j\boldsymbol{\beta}_{\mathrm{TX},n}(\phi_q)\cdot\left(\mathbf{r}'-\mathbf{r}_s^c\right)}\; T_q(\beta_{\mathrm{TX},n}, |\mathbf{r}_{so}^{cc}|, \phi_{so}^{cc})\; e^{-j\boldsymbol{\beta}_{\mathrm{TX},n}(\phi_q)\cdot\left(\mathbf{r}-\mathbf{r}_o^c\right)}, \tag{38}$$

is fulfilled, is computed. This can be done by first applying formula (32), which leads to a quite accurate estimate for $Q_{\mathrm{TX},n}$ that might still be slightly too large. Therefore, in a second step, $Q_{\mathrm{TX},n}$ can be gradually decreased while (37) is checked, as such leading to the desired, minimal $Q_{\mathrm{TX},n}$.

Table 2
Characteristics of the levels used in Fig. 6. For $|\mathbf{r}_{so}^{cc}| < 3\lambda_0$ a classical evaluation technique needs to be adopted.

level	R	$\min(\lvert\mathbf{r}_{so}^{cc}\rvert)$	$\max(\lvert\mathbf{r}_{so}^{cc}\rvert)$	number of modes needed for $d_0=3$	number of modes needed for $d_0=6$	number of modes needed for $d_0=9$
1	$\lambda_0/4$	$3\lambda_0$	$6\lambda_0$	17	26	34
2	$\lambda_0/2$	$6\lambda_0$	$12\lambda_0$	12	16	21
3	λ_0	$12\lambda_0$	$24\lambda_0$	9	11	14
4	$2\lambda_0$	$24\lambda_0$	$48\lambda_0$	6	8	9

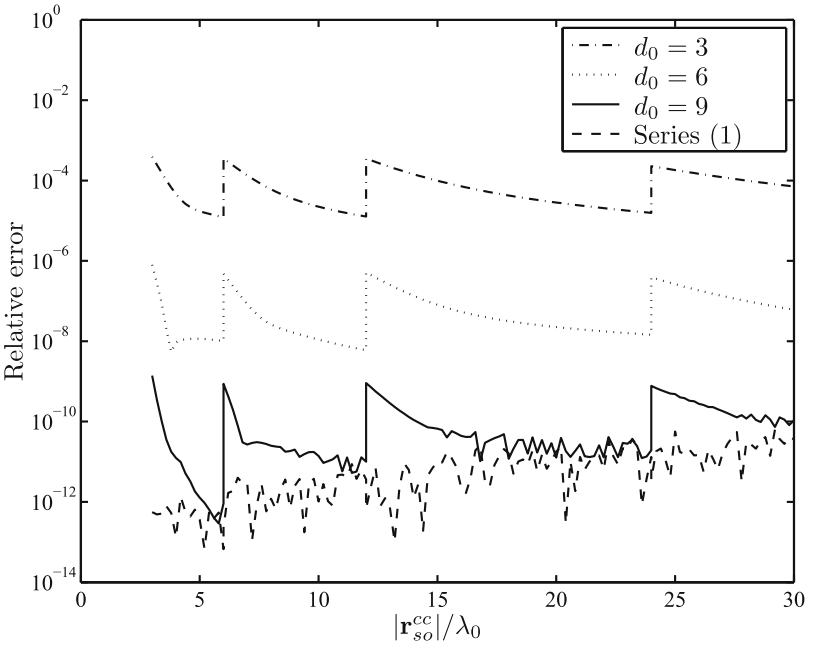

Fig. 6. Numerical accuracy of $G^A(|\mathbf{r}|\mathbf{r}'|)$, using (6) and (1), compared with (34) as a function of $|\mathbf{r}_{so}^{cc}|$ and for three different target accuracies 10^{-d_0}.

(iv) If in the previous step $Q_{\mathrm{TX},n}$ drops below zero, this means that the mode under consideration is not required to obtain the desired accuracy 10^{-d_0}. This mode will then no longer be used.

Now this approach is verified for the air-substrate as defined before. We consider four different levels in the MLFMA. At each level the source and observation are placed at the edge of the groups, i.e. at $\mathbf{r}' = (0, R, d)$ and $\mathbf{r} = (2(B+1)R, -R, d)$, respectively, where $2(B+1)R = |\mathbf{r}_{so}^{cc}|$, i.e. the distance between the two groups (see also Fig. 2). The characteristics of the levels are summarized in Table 2. In Fig. 6 the relative accuracy for $G^A(\mathbf{r}|\mathbf{r}')$ is given for three different target accuracies 10^{-d_0} and as a function of the distance $|\mathbf{r}_{so}^{cc}|$ between the center of the source and observation group. The different levels are clearly visible. Within one level, the number of modes is kept constant. It is clear from Fig. 6 that the above described algorithm to select the number of samples for each mode, leads to a controllable accuracy for the Green function in the PML-MLFMA. Also in Fig. 6, the maximal attainable accuracy is shown, which is given by the accuracy of the decomposition (1). This accuracy is approximately 11 digits, which is obtained by using $M = 50$ modes. Note that the results for $G^V(\mathbf{r}|\mathbf{r}')$ are not shown, as for this special configuration with $\epsilon_r = \mu_r = 1$, the results are exactly the same.

A last important remark has to be made. The above example, using the air-substrate, is definitely not the best case scenario. For a 'realistic substrate', with e.g. $\epsilon_r > 1$ and $\mu_r = 1$, there is always a TM-polarized surface wave present with $k_0 < \beta_{\mathrm{TM},1} < k_0\sqrt{\epsilon_r}$. Since this surface wave will dominate the accuracy of the Green function, this TM-polarized mode is used as a reference in formula (37), leading to very good results. Although it would be very hard to prove that the above proposed method to control the Green function's accuracy works for any possible configuration, many tests have shown that this is the case. A counterexample has not been found so far.

4. Conclusions

In this paper, the error controllability of the crux of the PML-MLFMA, viz. the pertinent layered medium Green functions, has been thoroughly investigated. In the PML-MLFMA, the Green functions are written as a series expansion of modes. Each mode corresponds to a (lossy) 2-D homogeneous space Green function, which is further decomposed into a set of plane waves. By rigorously deducing upper bounds for the required sampling rate of these plane wave decompositions, it is shown that the spectral content of the radiation patterns of each mode in the series expansion is quasi-bandlimited, allowing to sample them with a controllable accuracy. These new upper bounds are immediately applicable in 2-D MLFMAs, especially when the homogenous background medium is lossy. Next, these new formulas were used to develop a heuristic approach that allows to control the error of the layered medium Green functions that constitute the core of the PML-MLFMA. Both the upper bounds and the heuristic approach were tested by means of several numerical experiments, clearly demonstrating their validity and capabilities.

References

[1] V. Rokhlin, Rapid solution of integral equations of scattering theory in two dimensions, J. Comput. Phys. 36 (2) (1990) 414–439.
[2] N. Engheta, W.D. Murphy, V. Rokhlin, M.S. Vassiliou, The fast multipole method (FMM) for electromagnetic scattering problems, IEEE Trans. Antennas Propag. 40 (6) (1992) 634–641.
[3] C.C. Lu, W.C. Chew, A multilevel algorithm for solving a boundary integral equation of wave scattering, Microwave Opt. Technol. Lett. 7 (10) (1994) 456–470.
[4] W.C. Chew, J.-M. Jin, E. Michielssen, J. Song, Fast and efficient algorithms in computational electromagnetics, Artech House, Boston, USA, 2001.
[5] B. Hu, W.C. Chew, E. Michielssen, J.S. Zhao, Fast inhomogeneous plane-wave algorithm for the fast analysis of two-dimensional scattering problems, Radio Sci. 34 (4) (1999) 759–772.
[6] B. Hu, W.C. Chew, Fast inhomogeneous plane wave algorithm for electromagnetic solutions in layered medium structures: Two-dimensional case, Radio Sci. 35 (1) (2000) 31–43.
[7] B. Hu, W.C. Chew, Fast inhomogeneous plane wave algorithm for scattering from objects above the multilayered medium, IEEE Trans. Geosci. Remote Sensing 39 (5) (2001) 1028–1038.
[8] J.P. Bérenger, A perfectly matched layer for the absorption of electromagnetic waves, J. Comput. Phys. 114 (2) (1994) 185–200.
[9] W.C. Chew, W.H. Weedon, A 3D perfectly matched medium from modified Maxwell's equations with stretched coordinates, Microwave Opt. Technol. Lett. 7 (13) (1994) 599–604.
[10] F. Olyslager, H. Derudder, Series representation of Green dyadics for layered media using PMLs, IEEE Trans. Antennas Propag. 51 (9) (2003) 2319–2326.
[11] F. Olyslager, Discretization of continuous spectra based on perfectly matched layers, SIAM J. Appl. Math. 64 (4) (2004) 1408–1433.
[12] D. Vande Ginste, H. Rogier, D. De Zutter, F. Olyslager, A fast multipole method for layered media based on the application of perfectly matched layers – the 2-D case, IEEE Trans. Antennas Propag. 52 (10) (2004) 2631–2640.
[13] D. Vande Ginste, E. Michielssen, F. Olyslager, D. De Zutter, An efficient perfectly matched layer based multilevel fast multipole algorithm for large planar microwave structures, IEEE Trans. Antennas Propag. 54 (5) (2006) 1538–1548.
[14] S. Ohnuki, W.C. Chew, Error analysis of the fast inhomogeneous plane wave algorithm for 2D free-space cases, Microwave Opt. Technol. Lett. 38 (4) (2003) 300–304.
[15] M.A. Saville, W.C. Chew, Error control for 2-D FIPWA in complex, homogeneous media, J. Electromag. Waves Appl. 20 (5) (2006) 567–581.
[16] S. Ohnuki, W.C. Chew, Numerical accuracy of multipole expansion for 2-D MLFMA, IEEE Trans. Antennas Propag. 8 (51) (2000) 1883–1890.
[17] K.A. Michalski, D. Zheng, Electromagnetic scattering and radiation by surfaces of arbitrary shape in layered media, Part I: Theory, IEEE Trans. Antennas Propag. 38 (3) (1990) 335–344.
[18] N. Faché, F. Olyslager, D. De Zutter, Electromagnetic and Circuit Modelling of Multiconductor Transmission Lines, Oxford University Press Inc., New York, 1993.
[19] J. Song, W.C. Chew, Error analysis for the truncation of the multipole expansion of vector Green's functions, IEEE Microwave Wireless Compon. Lett. 11 (7) (2001) 311–313.
[20] M.A. Abramowitz, I.A. Stegun, Handbook of mathematical functions, Dover Publications, Inc., New York, 1970.
[21] A. Erdélyi, W. Magnus, F. Oberhettinger, G. Tricomi, Higher Transcendental Functions, vol. 2, McGraw-Hill Book Company, Inc., New York, 1953.

[22] E.L. Lehmann, Theory of Point Estimation, Wadsworth & Brooks/Cole, 1991.
[23] W. Feller, An Introduction to Probability Theory and Its Applications, 3rd ed., vol. 1, Wiley, New York, 1968.
[24] R.M. Corless, G.H. Gonnet, D.E.G. Hare, D.J. Jeffrey, D.E. Knuth, On the Lambert-W function, Adv. Comput. Math. 5 (4) (1996) 329–359.
[25] N. Geng, A. Sullivan, L. Carin, Fast multipole method for scattering from an arbitrary PEC target above or buried in a lossy half space, IEEE Trans. Antennas Propag. 49 (5) (2001) 740–748.